

The Silicon Vertex Detector of the Belle II Experiment

J. Wiechczynski,^{r,*} K. Adamczyk,^r H. Aihara,^p S. Bacher,^r S. Bahinipati,^e J. Baudot,^d
P. K. Behera,^f S. Bettarini,^{j,k} T. Bilka,^b A. Bozek,^r F. Buchsteiner,^a G. Casarosa,^{j,k}
L. Corona,^k S. B. Das,^g G. Dujany,^d C. Finck,^d F. Forti,^{j,k} M. Friedl,^a A. Gabrielli,^{l,m}
B. Gobbo,^m S. Halder,ⁱ K. Hara,^{q,n} S. Hazra,ⁱ T. Higuchi,^o C. Irmeler,^a A. Ishikawa,^{q,n}
Y. Jin,^m M. Kaleta,^r A. B. Kaliyar,^a J. Kandra,^b K. H. Kang,^o P. Kodyš,^b T. Kohriki,^q
R. Kumar,^h K. Lalwani,^g K. Lautenbach,^c R. Leboucher,^c J. Libby,^f L. Martel,^d
L. Massaccesi,^{j,k} G. B. Mohanty,ⁱ S. Mondal,^{j,k} K. R. Nakamura,^{q,n} Z. Natkaniec,^r
Y. Onuki,^p F. Otani,^o A. Paladino,^{A,j,k} E. Paoloni,^{j,k} K. K. Rao,ⁱ I. Ripp-Baudot,^d
G. Rizzo,^{j,k} Y. Sato,^q C. Schwanda,^a J. Serrano,^c T. Shimasaki,^o J. Suzuki,^q
S. Tanaka,^{q,n} F. Tenchini,^{j,k} R. Thalmeier,^a R. Tiwary,ⁱ T. Tsuboyama,^q Y. Uematsu,^p
L. Vitale,^{l,m} Z. Wang,^p H. Yin,^a L. Zani,^{B,c} and F. Zeng^o (Belle-II SVD collaboration)

^aInstitute of High Energy Physics, Austrian Academy of Sciences, 1050 Vienna, Austria

^bFaculty of Mathematics and Physics, Charles University, 121 16 Prague, Czech Republic

^cAix Marseille Université, CNRS/IN2P3, CPPM, 13288 Marseille, France, ^Bpresently at INFN Sezione di Roma Tre, I-00185 Roma, Italy

^dIPHC, UMR 7178, Université de Strasbourg, CNRS, 67037 Strasbourg, France

^eIndian Institute of Technology Bhubaneswar, Bhubaneswar 752050, India

^fIndian Institute of Technology Madras, Chennai 600036, India

^gMalaviya National Institute of Technology Jaipur, Jaipur 302017, India

^hPunjab Agricultural University, Ludhiana 141004, India

ⁱTata Institute of Fundamental Research, Mumbai 400005, India

^jDipartimento di Fisica, Università di Pisa, I-56127 Pisa, Italy, ^Apresently at INFN Sezione di Bologna, I-40127 Bologna, Italy

^kINFN Sezione di Pisa, I-56127 Pisa, Italy

^lDipartimento di Fisica, Università di Trieste, I-34127 Trieste, Italy

^mINFN Sezione di Trieste, I-34127 Trieste, Italy

ⁿThe Graduate University for Advanced Studies (SOKENDAI), Hayama 240-0193, Japan

^oKavli Institute for the Physics and Mathematics of the Universe, University of Tokyo, Kashiwa 277-8583, Japan

^pDepartment of Physics, University of Tokyo, Tokyo 113-0033, Japan

^qHigh Energy Accelerator Research Organization (KEK), Tsukuba 305-0801, Japan

^rH. Niewodniczanski Institute of Nuclear Physics, Krakow 31-342, Poland

E-mail: wiechczynski@belle2.ifj.edu.pl

*Speaker

35 The Belle II experiment operating at the asymmetric-energy e^+e^- SuperKEKB collider, located in Tsukuba (Japan), has been collecting data since March 2019. Its excellent vertexing abilities are provided by the vertex detector, part of which is the silicon-strip vertex detector (SVD) that plays a crucial role in the charged-particle tracking close to the interaction point. The SVD has operated successfully and efficiently over the whole period of data taking so far. In this article, we briefly discuss its purpose, structure and basic description of the front-end electronics. The main quantities related to the SVD performance are presented. The foreseen increase in SuperKEKB luminosity will lead to higher background, so we describe its impact on the SVD performance. A quick overview of the radiation damage campaign is presented to show the predicted behaviour of the sensors subjected to high radiation, whose level is constantly monitored. We also discuss the ongoing software development to account for the high occupancy expected in the future. In particular, the utilization of the SVD hit time information is presented as a very important quantity to suppress off-time background hits and tracks. Finally, the work done during the first long shutdown of SuperKEKB is briefly described, during which a major upgrade of the pixel detector has been successfully done. Resumption of the beam operation is expected in early 2024.

Keywords: Silicon strip detector, Vertex detector, Tracking detector, Belle II

1. Introduction

The Belle II [1] experiment is dedicated to search for physics beyond the standard model at the intensity frontier. It operates at the SuperKEKB collider located at KEK, Tsukuba in Japan, providing asymmetric beams of 7 GeV electrons and 4 GeV positrons. In the accelerator's default operation regime, the center-of-mass energy is set to the $\Upsilon(4S)$ resonance, hence it produces a huge sample of B mesons via the $e^+e^- \rightarrow \Upsilon(4S) \rightarrow B\bar{B}$ process. So far, SuperKEKB achieved the highest instantaneous luminosity of $4.7 \times 10^{34} \text{ cm}^{-2}\text{s}^{-1}$, which is the current world record. The Belle II detector is a multipurpose spectrometer characterized by excellent vertexing capability and good hermeticity, which has accumulated 424 fb^{-1} to date, and its final goal is to collect a data sample of 50 ab^{-1} , that will be possible with a constant increase of the SuperKEKB instantaneous luminosity up to our final goal of $6 \times 10^{35} \text{ cm}^{-2}\text{s}^{-1}$.

Belle II is composed of various sub-detectors with the vertex detector (VXD) being the closest to the interaction point. It is divided into two further subsystems. The innermost part is the pixel detector (PXD), which is based on depleted field effect transistor pixel sensors. The PXD consists of two layers (numbered 1-2) and its main goal is the precise determination of the decay vertices. Outside the PXD is the silicon-strip vertex detector (SVD) [2] with four layers (numbered 3-6) that mostly extrapolates the measured tracks to the PXD, defining the so-called region of interest (ROI), which significantly reduces the amount of data recorded by the PXD. The SVD also performs standalone tracking for low-momentum charged particles and contributes to their identification by providing energy loss information.

2. SVD structure

Each SVD layer is composed of a number of double-sided silicon strip detectors (DSSDs) that are manufactured on an n-type bulk wafer with a thickness of about $300 \mu\text{m}$ (Figure 1). One side of the sensor is covered by the p-type silicon strips placed in parallel to the beam axis that determine the $r-\phi$ coordinates (distance from the z -axis and azimuthal angle, respectively), and the n-type strips are placed perpendicularly on the other side of the bulk, measuring the z coordinate (collinear to the electron beam). Figure 1 (left) shows a schematic picture of SVD layers and associated sensors with increasing numbering from the forward (FWD) to the backward (BWD) regions. Such structure is repeated along the azimuthal direction forming different ladders and the so-called windmill geometry of the SVD. The sensors differ depending on the layer and the region in which they are placed in the SVD. In the FWD part, for layers 4-6, they have a trapezoidal shape

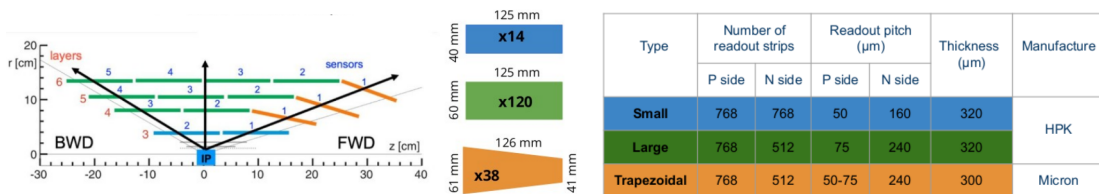


Figure 1: Schematic picture of SVD sensors forming different layers (left) and a table summarizing the parameters for each type of sensor (right).

67 and are slanted in the region that, due to the asymmetric beams, is characterised by the highest track
68 multiplicity. In addition, in layer 3 the sensors are smaller and contain more n-type strips than that
69 in layers 4-6. This also implies the readout pitch (distance between two readout strips) to be much
70 smaller for p-side strips with respect to the n-side. To improve spatial resolution, a floating strip is
71 placed between two readout strips on both p- and n-sides. The charge induced in the floating strip
72 is shared by the neighboring strips, reducing the effective strip pitch to half of the readout pitch.
73 The right table of Figure 1 summarises the sensor parameters. The SVD consists of 224 thousand
74 readout strips and 172 sensors with an active area of 1.2 m².

75 2.1 Fornt-end electronics

76 For the readout we use APV25 chips [3]. For the central part of SVD (except for layer 3), the
77 chips are attached directly to the DSSD sensors via flex circuits bent over the DSSD edge (Origami
78 concept). The edge sensors use hybrid boards located outside the active volume. The APV25 has
79 128 channels per chip and amplifiers that provide a shaping time of 50 ns. Radiation hardness
80 exceeds 100 Mrad and the power consumption is around 0.4 W/chip. The sampling frequency is 32
81 MHz and after the trigger's arrival we can collect six consecutive signal samples in total with the
82 multipeak mode. To account for higher luminosity in the future, we have introduced the so-called
83 "3/6 mixed acquisition mode", which allows switching between three and six samples recorded on
84 an event-by-event basis, based on the trigger type (and hence its time accuracy) for a particular
85 event. This mode, already prepared and tested, significantly reduces the data size, which can be
86 crucial in high background conditions.

87 3. SVD performance

88 Since the start of the operation we have observed very smooth performance of the SVD, with a
89 very few masked strips (less than 1%). Moreover, the environment has been stable and the evolution
90 of calibration constants is consistent with expectation. Also, the effects of radiation damage are
91 well under control.

92 Several quantities related to the SVD performance - sensor efficiency, signal-to-noise ratio, and
93 both spatial and time resolution - are constantly monitored. Regarding SVD sensor efficiency, the
94 values for all sensors are typically over 99% and they are also very stable over the whole period of
95 data taking. Clusters are formed from adjacent strips with significant signal and the charge collected
96 in a given cluster strongly depends on the incident angle of the track. Over time, we observe very
97 similar cluster charge in all the sensors once normalized to the track's length. For layer 4-5-6 on
98 the n-type strips we observe 10-30% loss of the signal due to the large pitch combined with the
99 presence of a floating strip. Another important quantity is the signal-to-noise ratio (SNR), which is
100 satisfactory for all 172 sensors. The SNR MPV is ranging from 13 to 30, depending on the sensor
101 position, due to the track incident angle with the sensor, and on the sensor side, with smaller SNR
102 for the p-sides, due to larger noise for the longer strip length. A small decrease of cluster SNR value
103 is observed in 2022 measurement, due to increased noise from radiation damage by approximately
104 20%-30%. In Figure 2 the distributions of cluster charge (left) and SNR (right) are presented,
105 where histograms representing the data collected in 2020 and 2022 are superimposed.

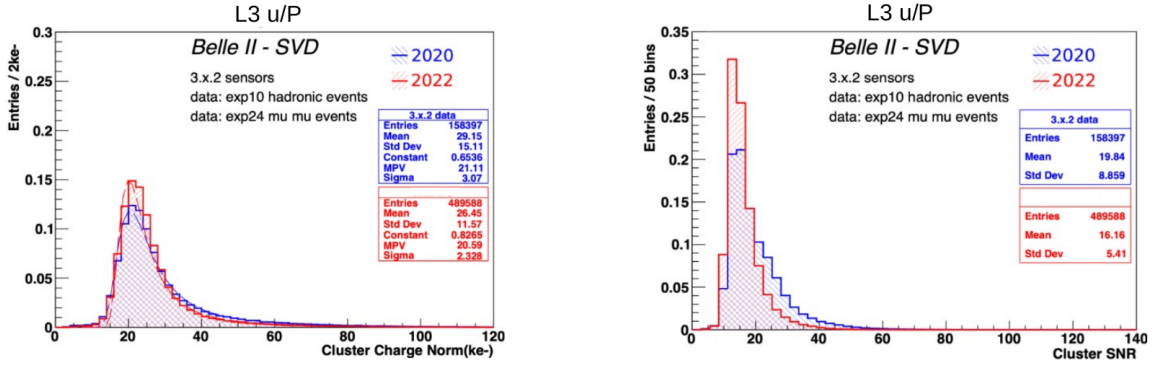


Figure 2: Distribution of cluster charge (left) and signal-to-noise ratio (right) for layer 3 (p-side). Comparison between data taken in 2020 (blue) and 2022 (red) is presented.

106 Both position and time resolution are very important metrics for excellent SVD performance.
 107 The position resolution measurement is based on the residuals, i.e., the clusters' positions with
 108 respect to the intercept of the unbiased tracks' extrapolation, and it is evaluated with a large sample
 109 of $e^+e^- \rightarrow \mu^+\mu^-$ decays. As shown in Figure 3, this quantity depends on the incident angle and is
 110 very stable during the period of the Belle II operation. As seen in Figure 3, the resolution for the
 111 n-side (left plot) is about two times worse with respect to that for the p-side, which is a result of the
 112 different pitch.

113 Hit time resolution is measured with respect to the event time of the collision provided by
 114 central drift chamber (CDC) and exhibits a very good resolution of less than 3 ns for the clusters
 115 associated to tracks. Using the average value of all the hits on a given track, the so-called "track-
 116 time" can be computed, slightly improving the time resolution. Furthermore, the "event-time" can
 117 be determined using all the clusters associated to selected tracks in an event. In such a way, the
 118 "event time" can be computed by the SVD with a resolution of the order of 1 ns, which is around
 119 2000 times faster with respect to the CDC-based computation. This feature will be especially
 120 important in the higher luminosity environment, as it can significantly speed up the reconstruction
 121 process at the high-level trigger.

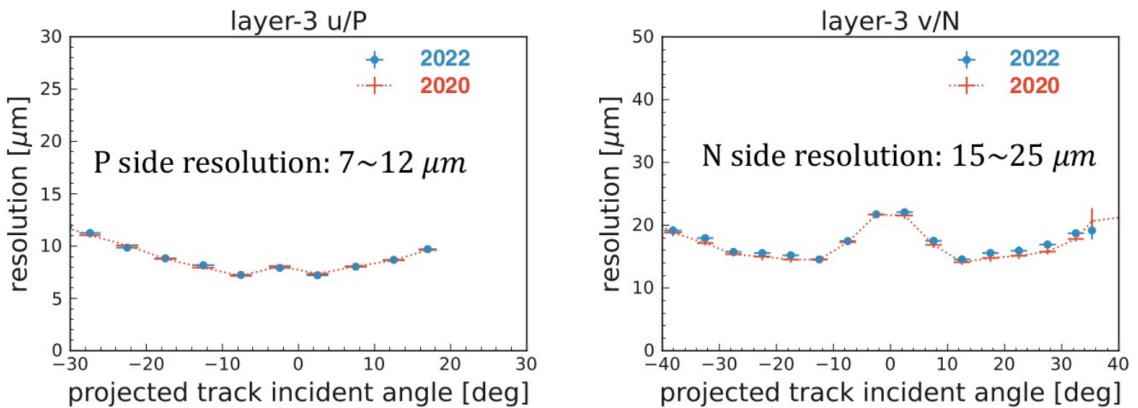


Figure 3: Distributions of position resolution for p-side (left) and n-side (right) as a function of the track incident angle. A comparison between data taken in 2020 (dots) and 2022 (dotted lines) is presented.

122 4. Radiation effects

123 In the high-energy physics experiments, the effects from radiation damage coming from ma-
 124 chine related background is a major factor that deteriorates the sensor performance with time. The
 125 SVD accumulated dose is constantly measured using data from diamond sensors that are mounted
 126 on the IP beam pipe, and the corresponding level of the equivalent neutron fluence is evaluated using
 127 the ratio of equivalent neutron fluence to dose estimated from Monte Carlo simulation. Several
 128 effects related to radiation damage must be taken into account. A linear increase of the leakage
 129 current as a function of radiation damage is observed in the sensors, as expected from the bulk
 130 damage described by the NIEL model [4], and shown in Figure 4 left. The sensor current is shown
 131 as a function of the accumulated dose for one of the layer 3 sensors most exposed, that received
 132 about 70 krad to date, corresponding to about 1.6×10^{11} neq. So far, this increase has had a
 133 negligible contribution to the noise because of both the small leakage current and the short APV25
 134 shaping time. The rate of the leakage current increase measured is consistent with the experience
 135 from other experiments working with similar detectors and in comparable conditions [5]. However,
 136 we expect some significant impact on the strip noise due to the sensor leakage current, and hence
 137 a deterioration in SNR, for the dose of ~ 6 Mrad, which is thus considered as SVD dose limit
 138 to preserve optimal performance. The strip noise for unirradiated modules is dominated by the
 139 interstrip capacitance. During the operation we have observed an increase in its value of about 20%
 140 (30%) for n-side (p-side), due to effects of surface radiation damage that increases the inter-strip
 141 capacitance, but it is expected to saturate, as also visible in Figure 4 center.

142 Another relevant effect of the bulk radiation damage is the impact on depletion voltage.
 143 The expected future radiation levels at the nominal luminosity, of about 0.35 Mrad/year and $8 \times$
 144 10^{11} neq/cm²/year, are affected by large uncertainty due to the machine evolution as well as a
 145 possible redesign of the interaction region. To better explore the possible effects of bulk damage in
 146 the SVD sensors after bulk type inversion, an irradiation campaign was conducted in July 2022 at
 147 ELPH, Tohoku University. Several SVD sensors have been exposed to a 90 MeV electrons beam,

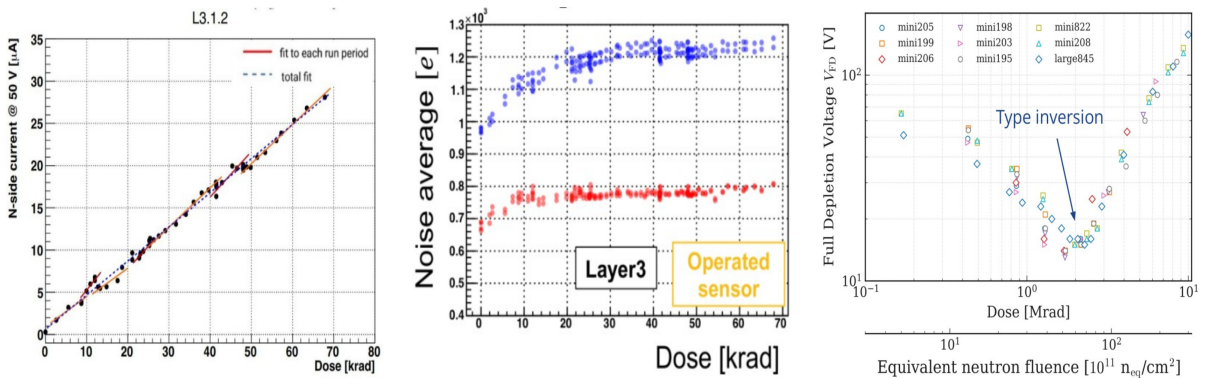


Figure 4: Left plot: Leakage current as a function of the accumulated dose; Center plot: the average noise level as a function of the accumulated dose for the p-side (blue dots) and n-side (red dots); Right plot: full depletion voltage as a function of the accumulated dose with the type inversion observed at 2 Mrad.

148 up to 10 Mrad, corresponding to an equivalent neutron fluence of 3×10^{13} $n_{\text{eq}}/\text{cm}^2$. The decrease
149 of the depletion voltage has been observed up to the point of bulk type inversion, which occurred at
150 2 Mrad ($\sim 6 \times 10^{12}$ $n_{\text{eq}}/\text{cm}^2$), after which the depletion voltage started to increase again (Figure 4
151 right). Detailed measurements, whose results will be shortly published, confirmed that the sensors
152 will still work fine after the type inversion, which meets our expectation for these types of silicon
153 detectors. Since the beginning of the detector operation, we have not observed any change in the
154 depletion voltage in the sensors installed in the SVD, as expected due to the small accumulated
155 equivalent neutron fluence so far, below 2×10^{11} $n_{\text{eq}}/\text{cm}^2$. Considering all these results, the dose
156 limit of 6 Mrad and the extrapolation of the background levels quoted above, the SVD has a wide
157 safety margin for the accumulated radiation damage even after 10 years of the operation at the target
158 luminosity.

159 5. High background scenario and related software/hardware developments

160 With the increase of the luminosity and the expected larger machine related background, the
161 SVD occupancy will also increase and a deterioration of the tracking performance is expected above
162 certain levels. So far, the average hit occupancy is 0.5% for layer 3, which does not degrade the
163 performance. Nonetheless, the background extrapolation for different future scenarios has been
164 performed with detailed simulations of the various contributions (beam-gas, Toushek, etc.) and
165 applying appropriate data-simulation scale factors [6]. These studies predict that for the nominal
166 luminosity we can reach an occupancy in layer 3 very close to the limit of 4.7%, above which the
167 tracking performance deteriorates. These predictions have large uncertainties coming from poorly
168 known machine evolution in the future, with a possible redesign of the interaction region. In the
169 most conservative scenario, the layer-3 occupancy can increase up to $\sim 8.7\%$, which is far beyond
170 the modest tracking performance. Such a scenario motivates us to develop the SVD reconstruction
171 software, as well as to seriously consider the VXD upgrade [7], since the safety factor might be too
172 small to ensure good quality data. The technology assessment related to this hardware upgrade is
173 currently ongoing.

174 An important effort related to the software development is the utilization of the hit time
175 information from the SVD. The real signal hits come from well-triggered collisions, but the SVD
176 acquisition window (~ 100 ns) is much wider with respect to the SuperKEKB bunch spacing (6 ns).
177 Therefore, we need to cope with many off-time hits related to the beam-induced background or
178 background from the other bunches. The current selection is based on two requirements: a) time
179 difference between p- and n-side cluster, $|t_p - t_n| < 20$ ns, and b) the absolute value of the cluster
180 time, $|t_{p,n}| < 50$ ns. These criteria reject the majority of the background hits retaining above 99% of
181 the signal, and based on them the SVD occupancy limit for layer 3 can be set at 4.7%. Recently, a
182 more effective background suppression method has been developed in the form of so-called “SVD
183 grouping”. It is based on an event-by-event classification of the clusters by their time, so the
184 clusters belonging to tracks from the same collisions are collected in the same group. Clusters
185 from the different collisions or beam background will be placed in the other groups; finally, only
186 the clusters belonging to the priority group will be used for the tracking. This feature reduces the
187 fake rate (fraction of the fake tracks) by 16% for the high-background scenario. An additional fake
188 rate reduction can be achieved by applying the selection on the track-time to reject off-time tracks.

189 Finally, these improvements allow an increase of the SVD occupancy limit for layer 3 from 4.7% to
190 around 6%.

191 **6. Activities during the Long Shutdown 1**

192 Long shutdown 1 (LS1) started in May 2022 and one of the goals was to upgrade the VXD with a
193 new PXD. During the first data taking period, the second layer of PXD was only partially equipped,
194 and 5/6 of the azimuthal angle remained uncovered. The new PXD provides the full coverage,
195 which is beneficial for more precise vertexing. Hardware activities for the VXD uninstallation and
196 reinstallation were intense: after the VXD extraction from Belle II, the SVD was detached from
197 the old PXD (May 16-17, 2023), then the new PXD was attached to the SVD (June 20-21, 2023)
198 and finally the complete VXD was installed in the Belle II detector. The whole delicate procedure
199 had neither major problems nor caused any damage. In the period of September 12 - October 1,
200 2023, the VXD commissioning was performed to confirm the PXD and SVD performance, and
201 also to check the impact from the increased PXD power consumption and possible increase in
202 the temperature on the sensor leakage current. From September 21, several cosmic runs with no
203 magnetic field were taken to check the performance and compare them with corresponding ones
204 for 2022 data samples. We observed no issues, in particular the noise distributions over readout
205 channels remained basically unchanged as well as SNR for the clusters associated to the tracks, with
206 stable excellent efficiency for all the sensors.

207 **7. Conclusions**

208 To conclude, SVD has successfully operated since March 2019 with very smooth performance
209 and without major problems. Its good vertexing quality has been confirmed by many physics
210 measurements, in particular those related to the lifetime analyses e.g. Ref. [8]. Some radiation
211 damage effects were observed, but without any impact on the performance so far.

212 However, the extrapolated background level indicates that the occupancy in the SVD can exceed
213 the current limit that guaranties good tracking performance. Hence, several software improvements
214 are being implemented to account for high background conditions. In particular, exploitation of
215 the SVD hit time is of major importance. Alongside, a VXD upgrade is also under discussion to
216 increase robustness against high background and to match a possible new interaction region.

217 The VXD reinstallation at Belle II with complete PXD has been successfully done during the
218 LS1, followed by successful VXD commissioning with cosmic data. The beam operation is planned
219 to resume in early 2024.

220 **References**

- 221 [1] T. Abe et al., Belle II Technical Design Report, arXiv:1011.0352 (2010).
222 [2] K. Adamczyk et al., JINST **17**, P11042 (2022).
223 [3] M. J. French et al., Nucl. Instrum. Meth. A **466**, 359 (2001).

- 224 [4] G. Lindstrom et al., Nucl. Instrum. Meth. A **465**, 60-69 (2000).
225 [5] B. Aubert et al., Nucl. Instrum. Meth. A **729**, 615 (2013).
226 [6] A. Natochii et al., Nucl. Instrum. Meth. A **1055**, 168550 (2023).
227 [7] M. Babeluk et. al., Nucl. Instrum. Meth. A **1048**, 168015 (2023).
228 [8] F. Abudinén et al., Phys. Rev. Lett. **130**, 071802 (2023)